Materials Science

http://www.aimspress.com/journal/Materials

AIMS Materials Science, 5(6): 1199–1213.
DOI: 10.3934/matersci.2018.6.1199
Received: 18 September 2018
Accepted: 11 November 2018
Published: 23 November 2018

Research article

Porous high-T_c superconductors and their applications

Michael R. Koblischka[1,2,*] **and Anjela Koblischka-Veneva**[1,2]

[1] Experimental Physics, Saarland University, P. O. Box 151150, 66041 Saarbrücken, Germany

[2] Superconducting Materials Laboratory, Department of Materials Science and Engineering, Shibaura Institute of Technology, 3-7-5 Toyosu, Koto-ku, Tokyo 135-8548, Japan

[*] **Correspondence:** Email: m.koblischka@mx.uni-saarland.de; Tel: +496813024555; Fax: +496813023790.

Abstract: Porous high-T_c superconducting materials offer several important benefits as compared to standard-type samples including an easy scalability towards large sample sizes, an easier oxygenation process and reduced weight. Due to these advantages, several different approaches to develop such samples were carried out in the literature. In this contribution, we present the microstructures and the physical properties of superconducting foams of $YBa_2Cu_3O_7$ and fabric-like, nanowire networks of $Bi_2Sr_2CaCu_2O_8$. Further, we discuss the properties of such samples concerning both the physical parameters and the respective microstructures and give an overview about possible applications.

Keywords: high-T_c superconductors; foams; nanowire fabrics; microstructure; magnetization; critical currents

1. Introduction

Superconducting samples are commonly prepared in the form of wires (tapes), bulks and thin films, depending on the desired type of application [1–3]. All these methods have the common goal to achieve a texture in the material, which leads to higher critical current densities and hence, to better superconducting properties. The consequence out of this are methods being applied which demand dedicated apparatuses and several processing steps and are, therefore, costly and time-consuming [4]. A second limit is the scalability of the product size, which is especially a problem for the bulk samples employed in levitation systems. The size of such superconducting samples reaches commonly to date only 5 cm in diameter, and 10 cm diameter samples are rarely claimed [5–7]. The size, however, determines the amount of magnetic field which can be trapped in the sample [8]. The larger the sample size, the longer the required oxygenation process will take (this can reach at the moment several weeks time). The oxygenation process also leads to (micro-)cracking, which severly reduces the mechanical

stability of the sample [9]. In the case of thin films, the evaporation chambers pose a size limit of the samples, and superconducting tapes using processes to reach long lengths, but the width is strictly limited. Altogether, samples with large lateral extensions are difficult to be prepared.

A possible way out of this situation are porous high-T_c superconductors. The pores in such samples enable the flow of oxygen throughout the sample in the oxygenation process and the required diffusion length is considerably reduced. In the application, the liquid coolant (e.g., liquid nitrogen) may also flow through the sample and not only around it, so the cooling process will be much more effective due to the small size of the superconducting elements (which helps to avoid formation of hot-spots in transport applications), and thus again reducing the costs of applying superconductors. Furthermore, the porous structure can be designed so that mechanical stability is even improved, and finally, porous materials have less weight and lower material content, which can be both important factors in applications. Now, for the preparation of porous high-T_c superconducting materials, several different approaches can be already found in the literature, including true porous materials like bulks with and without chemical additions [10–13], foams [14, 15], cloths [16], nanowire network fabrics [17–27] and artificially porous bulks where holes were machined into an otherwise regular bulk sample [28]. The foams were typically prepared using $YBa_2Cu_3O_7$ combined together with the infiltration (IG) process, whereas nanowires and nanowire fabrics were already prepared using (La,Sr)CuO_4 [18, 21], $YBa_2Cu_3O_7$ (YBCO or 123) [17, 20, 22], and $Bi_2Sr_2CaCu_2O_8$ (Bi-2212) [23–27].

In this contribution, we will present the microstructures and the superconducting properties of two types of real porous samples, the superconducting YBCO foam, and the nanowire network fabrics of Bi-2212 prepared by means of electrospinning. Finally, we discuss possible applications of these porous high-T_c superconductor samples.

2. Experimental procedures

The fabrication of the porous high-T_c superconducting materials is described in the following section and in Refs. [14, 15] for the foams, and in Refs. [23–25] for the Bi-2212 nanowire network fabrics. The microstructures were investigated using optical microscopes (Keyence), a SEM (JEOL 7000F) operating at 20 kV, and a TEM (JSM-7000 F) operating at 200 kV with a LaB_6 cathode. The electric measurements were performed in an Oxford Instruments 10/12 T Teslatron cryostat. The measurements were controlled by a MatLab program operating a stabilized current source (Keithley 2400) and a voltmeter (Keithley 2100 multimeter). The magnetic characterization measurements were performed using a MPMS3 SQUID (Quantum Design) magnetometer with 7 T maximum field.

3. Foams and nanowire network fabrics

Figure 1 presents the two types of porous, high-T_c superconducting samples. Image 1a is a typical piece of a superconducting foam with dimensions of $5 \times 2 \times 2$ cm^3. On top of the sample, which was prepared at RWTH Aachen in the years 2000–2002 [14, 15], there is a piece of an YBCO cloth (which is itself converted from Y_2O_3 to YBCO in a separate preparation process [16]) together with a seed crystal in the sample center. The cloth is required to guarantee the seed crystal to remain on top of the foam in the following IG process to convert the green Y_2BaCuO_5 (211) phase into the final

YBCO high-T_c compound. Finally, the foam sample underwent an oxygen annealing process. Figure 1b gives a typical view of a fully reacted, nanowire network fabric sample. The material is extremely light-weight and brittle, but one can already see from this image, that a single electrospinning run can produce a relatively large-sized, superconducting sample.

Figure 2 presents the porous high-T_c superconductors in the intermediate stage after the first preparation step, and Figure 3 give the microstructures of the as-prepared samples.

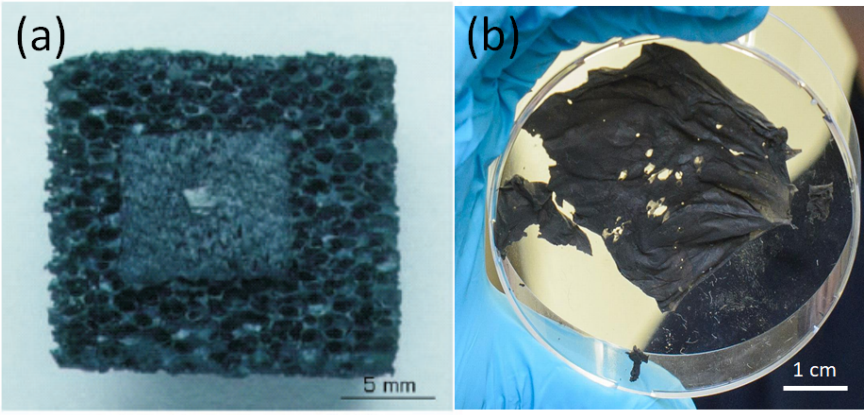

Figure 1. Fully reacted superconducting YBCO foam (a) and as-reacted Bi-2212 nanowire network fabric sample (b).

3.1. Superconducting foam samples

The superconducting foams are prepared in a two-step process. In the first step, a commercial polyurethane foam is converted to a ceramic, green 211 foam using a pre-prepared 211 slurry and followed by an appropriate heat treatment to burn out the polyurethane, the binder material(s) and to sinter the 211 powder. This green foam as depicted in Figure 2a undergoes an infiltration growth (IG) process to convert the 211 phase into the superconducting 123 phase. For this purpose, the green foam is placed above a liquid phase reservoir, and a seed crystal is placed on top of the foam sample in order to introduce an oriented growth of the 123 phase as in the case of standard YBCO bulks [2]. This arrangement is then subjected to a heat treatment. Finally, an oxygenation step is required to obtain the final product. The details about this preparation route can be found in Refs. [14, 15].

The resulting microstructure of the foam sample is presented in Figure 3a,b. Figure 3a gives a piece of a foam sample, broken away from the big foam piece for magnetic measurements. The photo is taken by an optical microscope (Keyence) using image processing to obtain an image with high imaging depth. From Figure 3a, one can directly recognize the pores and the individual struts forming the overall foam structure. Figure 3b presents an SEM image of a foam strut. The superconducting YBCO phase is the light grey matrix, and some 211 particles are embedded in this matrix. Also characteristic for the 123 matrix are the numerous stripes, which are grain boundaries as revealed by EBSD. The characterization of foam samples is still ongoing [29], as the complete understanding of the physical properties of the superconducting foam samples requires modelling approaches to simulate the 3D structure.

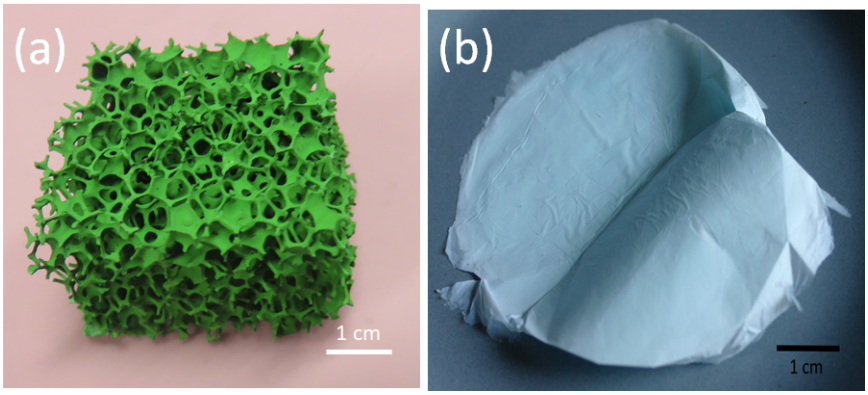

Figure 2. Porous superconductor samples in raw stage—the green phase (211) foam and white, unreacted polymer fabric containing the ceramic precursor material.

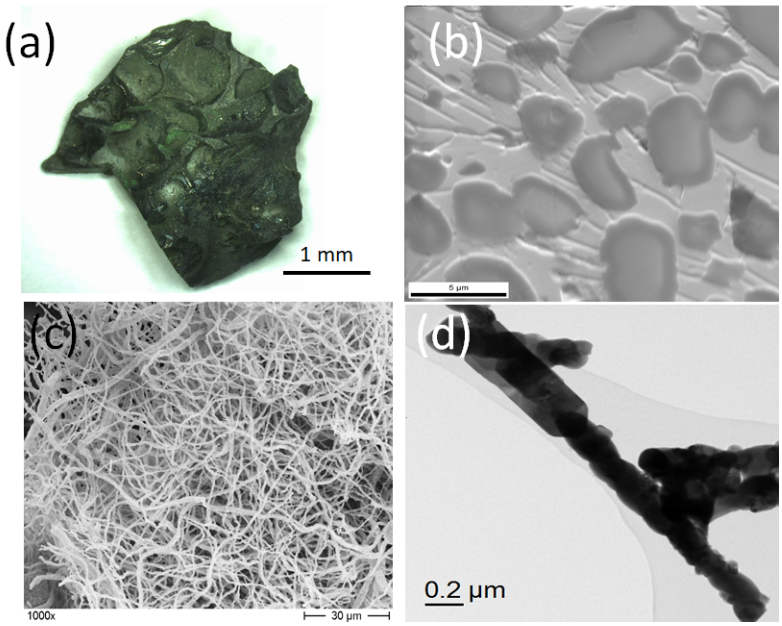

Figure 3. Microstructures of the foam sample (a) and (b), and of the nanowire network (c) and (d). (a) is an optical image of a foam piece consisting of several foam struts. (b) is an SEM image of an individual foam strut revealing the arrangement of the YBCO grains and the embedded 211 particles therein. (c) gives an SEM image of the as-reacted nanowire network fabric, showing the growth of the Bi-2212 grains (whiskers) along the original polymer nanowire. (d) presents a TEM image of a selected, thin Bi-2212 nanowire. Also shown are the interconnects between the nanowires.

3.2. Nanowire network fabrics

Nanowire network fabrics consist of long nanowires with lengths up to the micrometer range and diameters of ≈200–250 nm. Two methods are described in the literature to prepare such ceramic nanowire samples, electrospinning [30–32] and solution blow spinning [33]. With both methods, the

first fabrication step leads to polymer nanowires which contain the finely distributed ceramic precursor material. Figure 2b presents such an as-spun nanowire fabric. The sample has a white color, and the scale bar indicates the large size of the sample in this stage. It is important to note here that the following heat treatment to remove the organic material and to introduce the growth of the superconducting phase leads to a considerable shrinkage of the sample size. This must be taken into account when preparing samples for applications. Furthermore, the required temperatures to form the superconducting phase, which are typically in the range between 800 °C and 1100 °C, pose another problem: If the temperature is too high, the nanowire structure will collapse. Therefore, it is an essential issue to prepare the superconducting phase at temperatures as low as possible. Recent attempts in this direction have shown that this goal can be achieved [27], but on the price of having additional phases (as in the case of Bi-2212) or unreacted components.

In Figure 3c, an SEM image of the fully reacted Bi-2212 nanowire network fabric is given. A closer inspection reveals that the nanowires consist of elongated Bi-2212 grains which have grown along the original polymer nanowire. One can consider such a nanowire as a stack of several Bi-2212 whiskers, and the preferred growth direction is along the nanowire axis as revealed by an EBSD analysis using the transmission EBSD technique [34]. In some cases, these whiskers point out of the nanowire. Figure 3d gives a TEM image of an individual nanowire, together with an interconnect. One can see that this nanowire consists of only some Bi-2212 grains which have grown together. The diameter of the nanowire may be as small as the grain size. An important issue for the resulting superconducting properties of the nanowire network samples are the numerous interconnects between the individual nanowires. During the material growth, these interconnects are built up from grains of the superconducting phase, which finally enables the flow of superconducting currents through them. The consequence is a percolative current flow through the nanowire fabric sample throughout the entire sample perimeter [35]. As a consequence, the determination of current densities in such samples require modelling approaches as there are now contributions to the overall current flow of the superconducting grains (whiskers), of the grain boundaries between the grains and of the interconnects between the nanowires.

4. Magnetic and transport characteristics

Firstly, we look at the electric resistance measurements in the foam and the nanowire network samples. To both samples, electric contacts were fabricated using evaporated gold contacts and thin copper wires in a four-point configuration. Figure 4a shows the resistance of a foam sample as a function of temperature, measured for two different configurations, the current flow parallel to the c-axis, and the current flow parallel to the (a, b)-plane as presented in Ref. [36]. This graph demonstrates the texture introduced to the foam sample by employing the IG process and a seed crystal. Figure 4b presents the resistance, $R(T)$, measured on the nanowire network fabric in various applied magnetic fields ranging from 0 to 10 T ($H \perp$ sample surface, i.e., $H \perp j$). The superconducting transition is very broad, and shows two steps at all fields. Even at 10 T applied magnetic field, a zero-resistance state is reached at low temperatures, which indicates that transport currents can flow through the entire sample even at this high applied magnetic field. This graph directly proves that the interconnects and the grain boundary currents are quite strong at low temperatures. However, at temperatures above 40 K, the 2D character of Bi-2212 prohibits larger transport currents [37].

Now, we turn to the magnetization data. Figure 5a gives the temperature dependence of the magnetization, $M(T)$, after field-cooling (FC) in 1 mT applied field, field applied perpendicular to the sample surface of the foam sample. The foam piece is an extracted single strut, which has relatively small dimensions. In Figure 5a, only the ZFC curve is shown. The onset of superconductivity is obtained at 91 K like for bulk YBCO samples, and the transition in 10 mT applied field is somewhat broader (~12 K) as commonly observed for YBCO samples, but below 70 K, a stable and constant Meissner signal is reached. The broad transition is an indication of granularity effects, as oxygenation is not a problem for this type of sample.

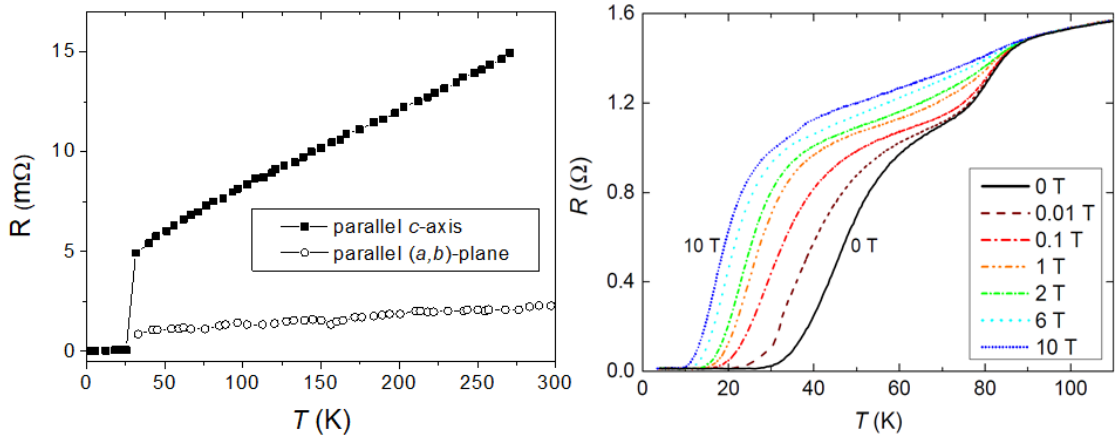

Figure 4. (a) $R(T)$ behavior of the foam sample for two configurations, current flow $\parallel c$ and $\parallel (a,b)$ (data from Ref. [36]) and (b) the $R(T)$ behavior in various applied magnetic fields ($H \perp$ sample surface) for the Bi-2212 nanowire network fabric. Reprinted (adapted) with permission from Ref. [23].

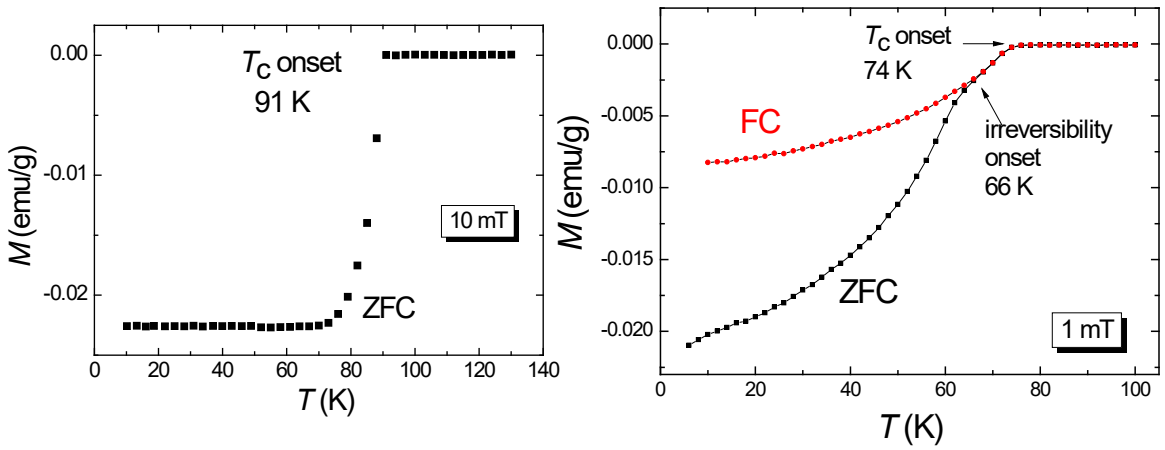

Figure 5. Temperature dependence, $M(T)$, of the foam sample (a) and of the Bi-2212 nanowire network fabric (b).

In the case of the nanowire network, several fabric pieces were employed to reach a large enough

signal—this procedure was necessary even when using a SQUID magnetometer for measurement. In this case, both FC and zero-field cooling (ZFC) was measured, enabling the observation of the onset of irreversibility (flux pinning). Overall, the superconducting transitions of the nanowire network fabric samples are found to be very broad, like in the case of the resistance measurements. However, in Figure 5b the onset of irreversibility in the Bi-2212 nanowire network sample at 66 K is clearly resolved; the onset of superconductivity is obtained at 74 K—just below the temperature of liquid nitrogen (77 K).

Let us now compare the superconducting transition temperatures, T_c, measured on various porous, high-T_c superconductors prepared in the literature and in our laboratory. Table 1 summarizes the data for T_c, together with some comment on the sample, the respective reference and the method employed to determine T_c.

Table 1. Superconducting transitions, T_c, and transition widths, ΔT_c, of the samples investigated here together with literature data. A dash in the table indicates that there is no information available. $M(T)$ indicates DC magnetic measurement, AC stands for AC susceptibility measurement, and $R(T)$ indicates resistance measurement. ES: electrospinning, SBS: solution blow spinning.

Sample type	T_c [K]	ΔT_c [K]	Ref.	meas. type	remarks
YBCO foam	91	1.7	[29]	$M(T)$	single foam strut
YBCO foam (large piece)	91.1	3.2	[29]	$M(T)$	piece containing pores
YBCO porous	93	3	[10]	$R(T)$	YBCO powder sintered with sucrose
YBCO porous	94	2.5	[11]	$R(T)$	YBCO powder sintered with sugar
YBCO cloths	90.5	5	[16]	AC	Y_2O_3 cloth converted to YBCO
YBCO with holes	91.5	1	[28]	$M(T)$	machined holes in bulk
Bi-2212 porous	94.5	5	[12]	AC	melt-textured Bi-2212 with C-nanotubes
Bi-2223 porous	105	3	[13]	$R(T)$	foam-like network of Bi-2223 crystallites
(La,Sr)CuO_4 nanowires	20	15	[18]	$M(T)$	ES, network fabric of round nanowires
(La,Sr)CuO_4 nanoribbons	29.3/13.9	-	[21]	$M(T)$	ES, thin, flat nanowires, 2 transitions
Bi-2212 nanowires	78.7	~50	[19]	$M(T)$	ES, network fabric of nanowires
Bi-2212 nanowires	84	20	[23]	$R(T)$	ES, network fabric of nanowires
	75	20	[24]	$M(T)$	
Bi-2212 nanowires + Pb	83.7	~50	[25]	$M(T)$	ES, network fabric of nanowires
Bi-2212 nanowires	81.6/78.6	–	[26]	$M(T)$	SBS, network fabric of nanowires
Bi-2212 nanowires + Li	74	~50	[27]	$M(T)$	ES, network fabric of nanowires
YBCO nanowires	92	~50	[17]	$M(T)$	ES, network fabric of nanowires
YBCO nanowires	91.7	~50	[20]	$M(T)$	ES, network fabric of nanowires
YBCO nanowires	–	–	[22]	$M(T)$	SBS, network fabric of nanowires

As one can see from Table 1, the superconducting transition temperatures of the porous YBCO samples range between 90.5 K and 94 K, which is similar to the commonly prepared bulks or thin films of the similar composition. The LSCO nanowires and nanoribbons show a lower T_c as the bulk materials, and T_c was even found to depend on the nanowire shape. This effect is likely due to the nanometric size of the wires, so effects like phase slip can take place reducing the measured T_c. The

Bi-2212 nanowires all exhibit lower transition temperatures as the respective bulks, and also very broad superconducting transitions, ΔT_c. Here, the large amount of high-angle grain boundaries plays a considerable role. Interestingly, the porous Bi-2212 bulks with addition of carbon nanotubes exhibit an even higher T_c as the commonly prepared bulks or single crystals (~85 K). The same observation applies for the porous Bi-2223 samples and the porous YBCO prepared using an addition of sugar, so the incorporation of carbon into the superconducting matrix and at the grain boundaries increases the T_c. Overall, one can say that the superconducting transition temperature of the porous materials is close or even higher as found in the conventional materials, which is an indication that the easier oxygenation process of the porous materials helps to improve the superconducting properties.

The magnetization hysteresis loops of the foam sample (Figure 6a) are completely smooth curves, not showing any fishtail characteristic, which is otherwise often seen for pure YBCO material. Also, there is indication of asymmetry which is a consequence of granularity. These data are taken one a single piece of a foam strut. EBSD analysis of the sample reveals that the strut is not oriented in pure (001) direction, but two main orientations can be found, being about 30° off. The graph shows clearly that ±5 T field is not enough to reach the irreversibility field at temperatures below 77 K, so the irreversibility field, H_{irr}, of the foam sample is quite large, which the foam samples share with the IG-processed YBCO bulk samples [38]. The inset to Figure 6a presents a magnetization loop taken at 85 K, which reveals only a relatively weak superconducting signal being present in the sample.

The magnetization hysteresis loops of the nanowire network sample (Figure 6b) are also smooth curves, but a large irreversibility is only obtained at low temperatures, 5 K $\leq T \leq$ 30 K. Also here, there are clear indications of granularity (asymmetry) and there is an overlaid diamagnetic magnetization, which has to be removed from the data prior to calculate the current densities.

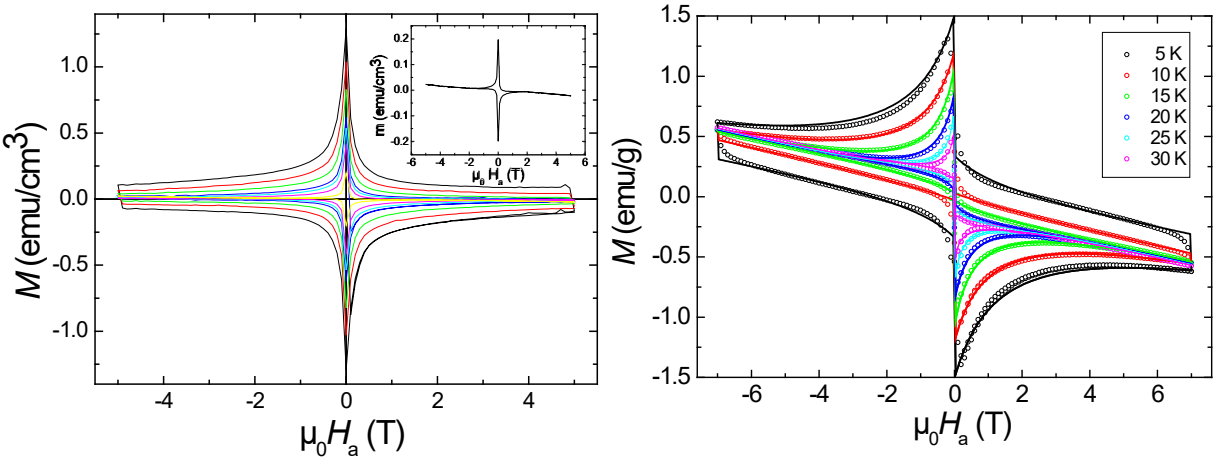

Figure 6. (a) Magnetization hysteresis data, $M(H)$, of the foam strut in the temperature range 60 K $\leq T \leq$ 85 K. The inset shows a MHL at 85 K in detail. (b) Magnetization data of the nanowire network fabric (b) at various temperatures in the temperature range 5 K $\leq T \leq$ 30 K. In (b), the datapoints represent the experimental data, and the solid lines are computed curves. Reprinted (adapted) with permission from Ref. [35].

Finally, Figure 7 gives the critical current density, j_c, as a function of applied field for the foam

sample (a) and the nanowire network (b). The current density was evaluated for the foam strut by applying the standard Bean model [39], whereas for the nanowire fabric, a more elaborated procedure is required to obtain j_c as the effective material cross section is a priori unknown. For this purpose, the extended critical state model was employed in Refs. [35, 40]. Using this approach, one can obtain a local current density, j_c, of the Bi-2212 grains, and an averaged critical current density, labeled here J_c. J_c corresponds to the current density flowing in a nanowire. The resulting current densities in the range 10^4–10^5 A cm^{-2} are reasonably large values, but it has to be mentioned here that the data of the foam sample are taken at temperatures between 60 K and 85 K, whereas the data for the nanowire fabric sample are measured at low temperatures between 5 K and 30 K. Nevertheless, the critical currents for the nanowire fabric sample are quite large when recognizing the small diameter of the nanowires; the j_c-data of the Bi-2212 grains are as high as in other samples of Bi-2212, e.g., powders or tapes [41].

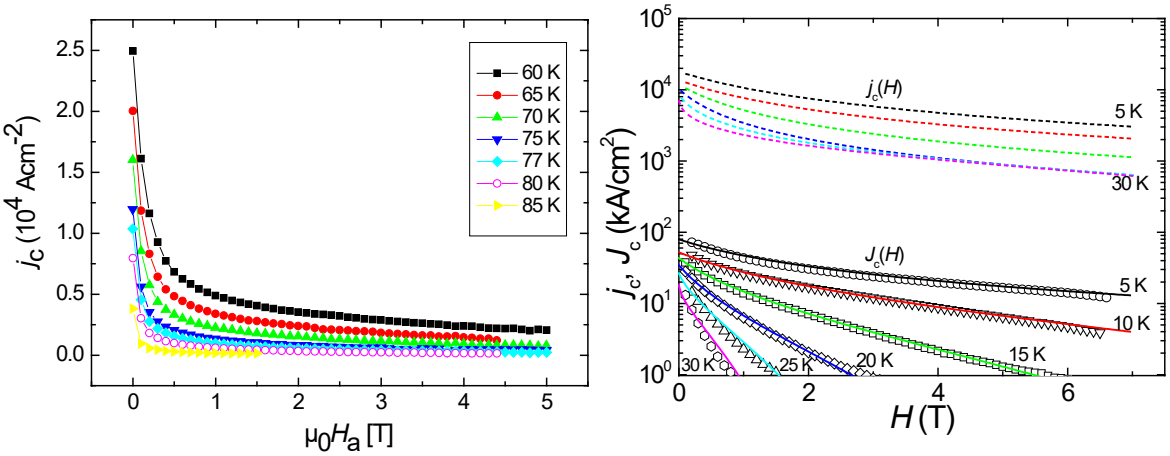

Figure 7. Critical current density, $j_c(H)$, of the foam (a) and the nanowire network fabric (b). (a) shows a steadily decaying current density with increasing field and no fishtail behavior. Reprinted (adapted) with permission from Ref. [39]. In (b), the lines are curves calulated using the extended critical state model (Dashed lines denote the local critical current density j_c of the Bi-2212 grains, and the solid lines represent the averaged critical current density J_c. The points are the critical current density obtained from evaluating the width of the experimental loops (Bean model). Reprinted (adapted) with permission from Ref. [35].

This observation is a common result for all porous superconducting materials—the grains within the porous material have the same superconducting properties as the ordinary bulk material. This defines the intragranular current density. The intergranular currents, however, are directly influenced by the porosity; either due to percolative current flow or due effects of trapped fields within the voids [42]. All this needs to be taken into account when deducing the critical current density of measurements of such porous samples. In an ideal case, the porous material would need to have a dominant texture. An attempt to fabricate such samples was made with the present YBCO foam samples, which underwent the infiltration growth process together with a seed crystal on top of the structure to introduce texture like in the melt-textured YBCO bulk samples. While X-ray analysis and also neutron diffraction demonstrated the achieved texture in the YBCO foam samples [43], the

magnetization data of individual foam struts still showed effects of granularity within the strut. However, the high irreversibility fields obtained for the YBCO foam samples are similar to those of IG-processed bulks, which demonstrates that the beneficiary microstructure (i.e., formation of small, nanometer-sized 211 particles as flux pinning sites) can be kept also in a porous structure. Here is certainly potential for further improving the performance of such samples in the future.

5. Possible applications

Concerning the applications of such porous samples, there are various possibilities considering the specific superconducting properties. All porous samples benefit from the fact that the oxygenation process and the cooling process are much more effective as compared to the bulk counterparts. Already the preliminary experiments to prepare these types of samples being carried out demonstrate the scalability, offering the unique possibility to prepare large-scale superconducting samples. The other central interest is the light weight of the porous superconductor samples. This offers a variety of possible applications, whereever the weight is an important issue, e.g., for rotating electric components as well as for applications in space. This is especially true for the nanowire network fabric samples—a magnetic shield constructed with such a light-weight material does not add additional weight to a given construction, but clearly improves the effectivity of the device. Already in the first publication on superconducting foams [14] it was discussed that superconducting foams may find applications that require efficient heat extraction from the superconducting components, e.g., in resistive fault current limiters [44]. Furthermore, foams are ideal materials for interconnected, reinforced composites with improved mechanical properties. Foams also allow for tailoring overall thermal or electrical behavior of the superconducting foam itself by further coating. Such coatings may also be employed to increase the mechanical stability as shown in Ref. [45] for metal-coated Al foams. It should also be noted that the shape of the foam samples like presented in Figure 1a was mainly selected to mimic the shape of bulk superconductors intended for trapped field applications, so one can imagine many different sample shapes optimized for other applications. This also applies for the porosity, which can be tuned employing different types of precursor foams. For the trapped field experiments, one even still needs to find the optimum configuration, as mainly the sample diameter is essential for maximizing the field trapping properties.

A goal for future developments is the processing of larger sample sizes, which will require the use of multiple seed crystals on such a large-sized sample. Similar experiments were already done in the literature on melt-proceesed bulk samples, so the basic know-how already exists [46]. As already mentioned, further treatments of the foam samples are possible, including coating the foams with metal overlayers or to fill the foams with polymers. Both approaches can be used to increase the mechanical strength of the samples, which is an essential issue for trapped field applications [5–7], but also thermal and electrical properties can be tuned in this way.

The nanowire network fabrics also provide the possibility to fabricate large-sized samples. However, the brittleness of this material hinders the use in applications. A possible way out of this dilemma is the fabrication of superconducting foils—embedding the fully reacted nanowire network into a suitable resin which can withstand the required low temperatures [47, 48]. As a result, a flexible superconducting foil can be created, which could easily cover also complicated shapes when being used as a magnetic shield. Such a foil type of sample is depicted in Figure 8b, which still maintains

the low weight of the original nanowire fabric. Furthermore, there are many possibilities to apply large-scale superconducting samples. One such idea is the superconducting carpet—a large-scale nanowire network with the extension of several tens of centimeters. Placed on a suitable substrate and cooled in flowing liquid nitrogen from the bottom side, such a superconducting carpet may be a base for floating magnets on which several objects can be carried (see Figure 9a).

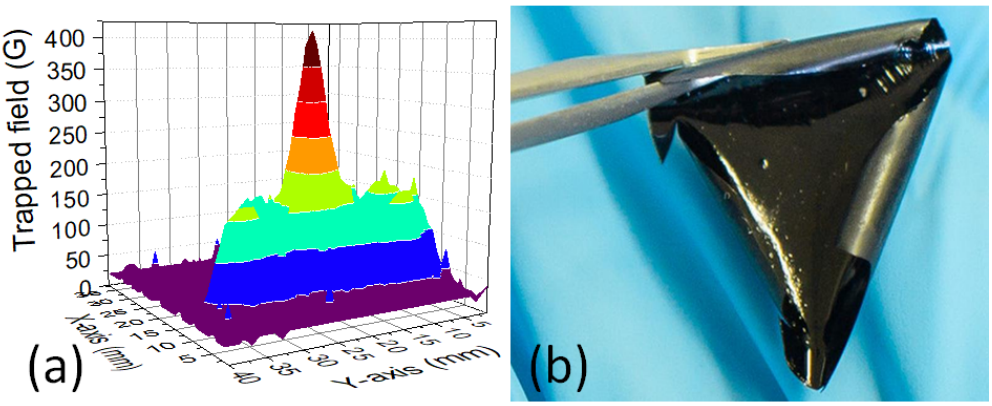

Figure 8. (a) Trapped field measurement on a superconducting foam, magnetized by field-cooling the foam with a 0.5 T permanent magnet, 77 K. (b) Flexible superconducting foil, consisting of a nanowire network fabric embedded in a resin which can withstand the necessary low temperatures.

Figure 9b gives a superconducting rail, which consists of a square tube filled with a long piece of superconducting foam. The tube enables the coolant to be sent through the sample, providing effective cooling. An object with magnets on its bottom can levitate above such a rail. For a practical application, several such rails will be required. This configuration quasi "inverts" the common levitation principle, but solves the otherwise existing cooling problem of the levitated object. All together, these arrangements depicted in Figure 9 may enable new forms of movements in industrial machinery, facilitating the placing of objects.

Such motion systems for industrial use are currently developed at FESTO AG [49], based on conventional, bulk high-T_c superconductors and permanent magnets. Having such a large scale superconducting carpet—which will form the base for the application and can be cooled from the bottom side—together with the ideas developed within their project, many more practical solutions may be devised, as now there is no size limit for the superconducting material. Interestingly enough, such a superconducting carpet may be realized by nanowire fabrics as well as foams.

Finally, Figure 9c presents fully reacted, donut-shaped nanowire fabrics. As the shaping of the as-spun polymer network is straightforward, such special shapes of the samples can easily be realized. After the heat treatment, the new shape is stable. Such a shaped nanowire network fabric can now be employed, e.g., as a light-weight magnetic shield. The field inside the hole of the donut can now be measured using a Hall probe setup. This possibility to produce superconducting samples of any shape

is an unique feature of the nanowire network fabrics, and together with the extremely low weight, this feature may offer interesting new types of applications.

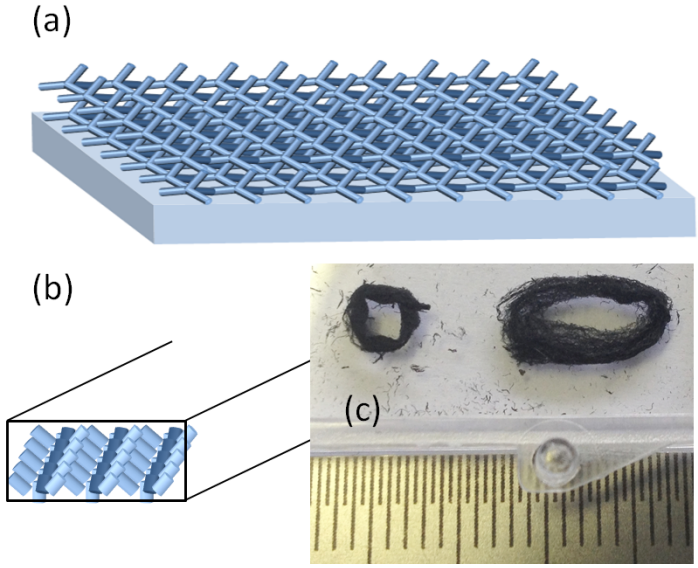

Figure 9. (a) "Superconducting carpet" (scheme), placed on a substrate. The cooling will take place from the bottom side when using a foil-type sample, or the coolant can be sent through the superconductor when using a foam. Several objects can be levitated above it at once, and manipulation can be easily done (e.g., by a robot arm). (b) Superconducting rail. In a square tube, a long foam sample may be placed. The coolant can be sent directly through the sample. (c) Fully reacted, donut-shaped nanowire network fabric samples.

6. Conclusion

We have shown several superconducting properties and the microstructures of high-T_c superconducting foams and of nanowire network fabric samples. The properties of these porous high-T_c superconductors are very interesting for a variety of applications. The possibility offered by both materials to upscale the sample size may bring forward several new types of applications of high-T_c superconductors. The measurements reveal that the intragrain currents of porous materials are as high as the standard-type samples, whereas the intergrain currents suffer from the existing grain boundaries, so these currents are smaller than in the normal samples. However, the high irreversibility fields of the YBCO foam samples show that the beneficiary microstructure can also be kept in porous HTSc samples. Therefore, the porous HTSc samples have potential for further improvement of the current densities when all recent developments of sample fabrication can be incorporated.

Acknowledgments

The authors thank G. Schmitz (ACCESS, RWTH Aachen) for giving insights to the foam preparation work. We also acknowledge the collaboration with D. Gokhfeld (Kirensky Institute of Physics, Krasnojarsk, Russia), C. Chang, T. Hauet (Institute Jean Lamour, Université de Lorraine,

Nancy, France), K. Berger, B. Douine (GREEN, Université de Lorraine, Nancy, France) and S. Pavan Kumar Naik, M. Muralidhar, M. Murakami (SIT, Tokyo, Japan). Further, we thank X. L. Zeng, A. Wiederhold, J. Schmauch (UdS) for the technical assistance. This work is financially supported by the projects Ko2323/8 (DFG), Ko2323/10 (DFG/ANR), SIT start-up grant and Volkswagen Foundation, which is gratefully acknowledged.

Conflict of interest

There is no conflict of interest.

References

1. Foltyn SR, Civale L, MacManus-Driscoll JL, et al. (2007) Materials science challenges for high-temperature superconducting wire. *Nat Mater* 6: 631–642.
2. Murakami M (1991) *Melt Processed High-Temperature Superconductors*, Singapore: World Scientific.
3. Scanlan RM, Malozemoff AP, Larbalestier DC (2004) Superconducting materials for large scale applications. *P IEEE* 92: 1639–1654.
4. Grant PM, Sheahen TP (1998) Cost projection for high temperature superconductors. *Applied Superconductivity Conference*, Palm Desert, CA.
5. Hull JR, Strasik M (2010) Concepts for using trapped flux bulk high-temperature superconductors in motors and generators. *Supercond Sci Tech* 23: 124005.
6. Tomita M, Murakami M (2003) High-temperature superconductor bulk magnets that can trap magnetic fields above 17 tesla at 29 K. *Nature* 421: 517–520.
7. Durrell JH, Dennis AR, Jaroszynski J, et al. (2014) A trapped field of 17.6 T in melt-processed bulk Gd-Ba-Cu-O reinforced with shrink-fit steel. *Supercond Sci Tech* 27: 082001.
8. Johansen TH (2000) Flux-pinning-induced stress and magnetostriction in bulk superconductors. *Supercond Sci Tech* 13: R121–R137.
9. Diko P (2004) Cracking in melt-grown RE-Ba-Cu-O single-grain bulk superconductors. *Supercond Sci Tech* 17: R45–R58.
10. Fiertek P, Sadowski W (2006) Processing of porous structures of $YBa_2Cu_3O_{7-\delta}$ high-temperature superconductor. *Mater Sci-Pol* 24: 1103–1108.
11. Fiertek P, Andrzejewski B, Sadowski W (2010) Synthesis and transport properties of porous superconducting ceramics of $YBa_2Cu_3O_{7-\delta}$. *Rev Adv Mater Sci* 23: 52–56.
12. Huang SL, Koblischka MR, Johansen TH, et al. (1997) Increased flux pinning in both pure and carbon-nanotube-embedded Bi-2212 superconductors. *Physica C* 282–287: 2279–2280.
13. Petrov MI, Tetyueva TN, Kveglis LI, et al. (2003) Synthesis, Microstructure, and the Transport and Magnetic Properties of Bi-Containing High-Temperature Superconductors with a Porous Structure. *Tech Phys Lett* 29: 986–988.
14. Reddy ES, Schmitz GJ (2002) Ceramic foams. *Am Ceram Soc Bull* 81: 35–37.

15. Reddy ES, Herweg M, Schmitz GJ (2003) Processing of Y_2BaCuO_5 foams. *Supercond Sci Tech* 16: 608–612.

16. Noudem JG, Reddy ES, Tarka M, et al. (2002) Electrical performance of single domain $YBa_2Cu_3O_7$ fabrics. *Physica C* 366: 93–101.

17. Zhang GQ, Lu XL, Zhang T, et al. (2006) Microstructure and superconductivity of highly ordered $YBa_2Cu_3O_{7-\delta}$ nanowire arrays. *Nanotechnology* 17: 4252–4256.

18. Li JM, Zeng XL, Mo AD, et al. (2011) Fabrication of cuprate superconducting $La_{1.85}Sr_{0.15}CuO_4$ nanofibers by electrospinning and subsequent calcination in oxygen. *CrystEngComm* 13: 6964–6967.

19. Duarte EA, Quintero PA, Meisel MW, et al. (2013) Electrospinning synthesis of superconducting BSCCO nanowires. *Physica C* 495: 109–113.

20. Duarte EA, Rudawski NG, Quintero PA, et al. (2015) Electrospinning of superconducting YBCO nanowires. *Supercond Sci Tech* 28: 015006.

21. Zeng XL, Koblischka MR, Hartmann U (2015) Synthesis and characterization of electrospun superconducting (La,Sr)CuO_4 nanowires and nanoribbons. *Mater Res Express* 2: 095022.

22. Rotta M, Zadorosny L, Carvalho CL, et al. (2016) YBCO ceramic nanofibers obtained by the new technique of solution blow spinning. *Ceram Int* 42: 16230–16234.

23. Koblischka MR, Zeng XL, Karwoth T, et al. (2016) Transport and magnetic measurements on $Bi_2Sr_2CaCu_2O_8$ nanowire networks prepared via electrospinning. *IEEE T Appl Supercon* 26: 1800605.

24. Koblischka MR, Zeng XL, Karwoth T, et al. (2016) Magnetic properties of electrospun non-woven superconducting fabrics. *AIP Adv* 6: 035115.

25. Zeng XL, Koblischka MR, Karwoth T, et al. (2017) Preparation of granular Bi-2212 nanowires by electrospinning. *Supercond Sci Tech* 30: 035014.

26. Cena CR, Torsoni GB, Zadorosny L, et al. (2017) BSCCO superconductor micro/nanofibers produced by solution blow-spinning technique. *Ceram Int* 43: 7663–7667.

27. Koblischka MR, Zeng XL, Laurent F, et al. (2018) Characterization of electrospun $Bi_2Sr_2CaCu_2O_{8+\delta}$ nanowires with reduced preparation temperature. *IEEE T Appl Supercon* 28: 7200505.

28. Noudem JG (2011) Developing of shaping textured YBaCuO superconductors. *J Supercond Nov Magn* 24: 105–110.

29. Nie Z, Lin Y, Tong Q (2017) Modeling structures of open cell foams. *Comp Mater Sci* 131: 160–169.

30. Wu H, Pan W, Lin D, et al. (2012) Electrospinning of ceramic nanofibers: Fabrication, assembly and applications. *J Adv Ceram* 1: 2–23.

31. Li D, McCann JT, Xia YN (2006) Electrospinning: A simple and versatile technique for producing ceramic nanofibers and nanotubes. *J Am Ceram Soc* 89: 1861–1869.

32. Huang ZM, Zhang YZ, Kotaki M, et al. (2003) A review on polymer nanofibers by electrospinning and their application in nanocomposites, *Compos Sci Technol* 63: 2223–2253.

33. Medeiros ES, Glenn GM, Klamczynski AP, et al. (2009) Solution Blow Spinning: A New Method to Produce Micro- and Nanofibers from Polymer Solutions. *J Appl Polym Sci* 113: 2322–2330.
34. Koblischka-Veneva A, Koblischka MR, Zeng XL, et al. (2018) TEM and electron backscatter diffraction analysis (EBSD) on superconducting nanowires. *J Phys Conf Ser* 1054: 012005.
35. Zeng XL, Karwoth T, Koblischka MR, et al. (2017) Analysis of magnetization loops of electrospun non-woven superconducting fabrics. *Phys Rev Mater* 1: 044802.
36. Noudem JG, Reddy ES, Schmitz GJ (2003) Magnetic and transport properties of $YBa_2Cu_3O_y$ foams. *Physica C* 390: 286–290.
37. Koblischka MR, Sosnowski J (2005) Temperature-depedendent scaling of pinning force data in Bi-based high-T_c superconductors. *Eur Phys J B* 44: 277–280.
38. Nakazato K, Muralidhar M, Koblischka MR, et al. (2014) Fabrication of bulk Y–Ba–Cu–O superconductors with high critical current densities through the infiltration-growth process. *Cryogenics* 63: 129–132.
39. Koblischka MR, Koblischka-Veneva A, Chang C, et al. (2018) Flux pinning analysis of superconducting YBCO foam struts. *IEEE T Appl Supercon* [In press].
40. Gokhfeld DM (2014) An extended critical state model: Asymmetric magnetisation loops and field dependence of the critical current of superconductors. *Phys Solid State* 56: 2380–2386.
41. Mikheenko PN, Uprety KK, Dou SX (2001) BSCCO, In: Cardwell DA, Ginley DS, *Handbook of superconductiing materials*, Bristol: IOP Publishing, 947–993.
42. Terent'ev KYu, Gokhfeld DM, Popkov SI, et al. (2011) Pinning in a Porous High-Temperature Superconductor Bi2223. *Phys Solid State* 53: 2409–2414.
43. Noudem JG, Guilmeau E, Chateigner D, et al. (2004) Properties of $YBa_2Cu_3O_y$-textured superconductor foams. *Physica C* 408–410: 655–656.
44. Tournier R, Beaugnon E, Belmont O, et al. (2000) Processing of large $Y_1Ba_2Cu_3O_{7-x}$ single domains for current-limiting applications. *Supercond Sci Tech* 13: 886–896.
45. Jung A, Diebels S, Koblischka-Veneva A, et al. (2013) Microstructural analysis of electrochemical coated open-cell metal foams by EBSD and nanoindentation. *Adv Eng Mater* 16: 15–20.
46. Goodfellow A, Shi YH, Durrell JH, et al. (2016) Microstructural evolution in multiseeded YBCO bulk samples grown by the TSMG method. *Supercond Sci Tech* 19: 115005.
47. Haupt SG, Riley GR, McDevitt JT (1993) Conductive polymer/high-temperature superconductor composite structures. *Adv Mater* 5: 755–758.
48. Shirbeny W, Hafez M, Mahmoud WE (2013) Synthesis and characterization of PVA/YBCO nanocomposite for improvement of solar energy conversion. *Polym Composite* 34: 587–591.
49. SupraMotion 2017: Superconductors for automatization. Brochure FESTO AG & Co KG. Available from: http:// www.festo.com/supra.

AIMS Press